Soft Matter

RSC Publishing

PAPER

View Article Online
View Journal | View Issue

Self-assembly of spherical colloidal particles with off-centered magnetic dipoles

Cite this: *Soft Matter*, 2013, **9**, 8904

Alexei I. Abrikosov,[a] Stefano Sacanna,[b] Albert P. Philipse[c] and Per Linse*[a]

Fluids of spherical colloids possessing an off-centered embedded magnetic dipole were investigated by using Monte Carlo simulations. Systems of colloids with different strengths and directions of the embedded dipole moment confined in a 2D space without and with an external magnetic field applied were considered. The fluids were characterized by radial distribution functions, angular distribution functions, cluster data, and energetic data. In the absence of an external field, the colloids form dimers and trimers at sufficiently large magnetic moment without the tendency of forming chains of colloids as appearing in systems with particles possessing a central magnetic dipole. In the presence of an external field, chains of colloids aligned in a zigzag fashion were formed for a field parallel to the plane of the particles, whereas the colloidal ordering was suppressed in the presence of a field perpendicular to that plane. The findings agree surprisingly well with the recent experimental observations on fluids containing spherical polymer colloids with embedded single-domain magnetic hematite cubes (S. Sacanna, L. Rossi, and D. J. Pine, *J. Am. Chem. Soc.*, 2012, **134**, 6112).

Received 14th September 2012
Accepted 18th July 2013

DOI: 10.1039/c3sm27128e

www.rsc.org/softmatter

1 Introduction

Over the past decade, the extent to which colloidal pieces of matter can be engineered to meet desired features has been unprecedented. Surface patches, anisotropic shapes, and reversible interactions can be designed to act in unison and animate microscopic building blocks.[1] At the same time, theoretical and numerical simulations facilitate the design process by predicting system energetics and revealing assembly pathways towards new exciting materials.[2–5] Rationally designed colloids have been shown to self-assemble into crystalline and quasicrystalline lattices,[6–8] chiral structures,[9,10] flexible clusters,[11] reversible colloidal-micelles[12] and chains.[13,14] Recently, the structure of fluids containing spherical particles with embedded off-centered magnetic dipoles with a dipole direction parallel to the vector from the center of the colloid to the dipole has been theoretically analyzed.[16–19]

Very recently, experiments have been reported on colloidal spheres with an embedded off-centered magnetic hematite cube.[15] The magnetic cubes[7] were enclosed in spherical colloids with the magnetic cube near the colloidal surface. Due to the off-centered dipole moment, the spheres reversibly form finite-size clusters in the zero-field that rearrange to dipolar chains in an external magnetic field.

Here, our aim is to simulate the self-assembly of spherical particles with off-centered dipoles and to make a comparison with the experimentally observed structures.[15] One important advantage of simulating model systems is that the direction and the strength of the (permanent) dipole moments can be systematically varied – a variation that in an experimental fluid is very difficult to achieve. Moreover, the direction of the dipole moment in the experimental hematite cube is not yet fully known; thus, the simulations could be used to investigate various scenarios for the direction of the off-centered magnetic moment and assess any consequences for the structure formation in zero field and with an applied external field. An important difference between the work by Kantorovich *et al.*[16] and by us is that we consider cases where the dipole direction is *not* parallel to the vector from the center of the colloid to the dipole, which most likely is the case in the experimental systems inspiring us.

2 Model

Fluids of magnetic colloids are here represented by a coarse-grained model. We restrict ourself to the case where the N particles are confined on a plane with the area A but still retain full 3D rotational ability (quasi-2D space), giving the particle number density $\rho_A = N/A$. The quasi-2D space was chosen to match the experimental setup by Sacanna *et al.*[15]

The particles are spherical with the hard-sphere radius R and possess the magnetic point dipole $\boldsymbol{\mu}$. As illustrated in Fig. 1, the dipole is located on the (local) z'-axis of the particle at distance sR, $0 \leq s < 1$, from the center of the particle and forming the angle β

[a]*Physical Chemistry, Department of Chemistry, Lund University, P.O. Box 124, S-221 00 Lund, Sweden. E-mail: per.linse@fkem1.lu.se*

[b]*Center for Soft Matter Research, Department of Physics, New York University, 4-6 Washington Place, New York, NY 10003, USA*

[c]*Van't Hoff Laboratory for Physical and Colloid Chemistry, Debye Institute for Nanomaterials Science, Utrecht University, Padualaan 8, 3584 CH Utrecht, The Netherlands*

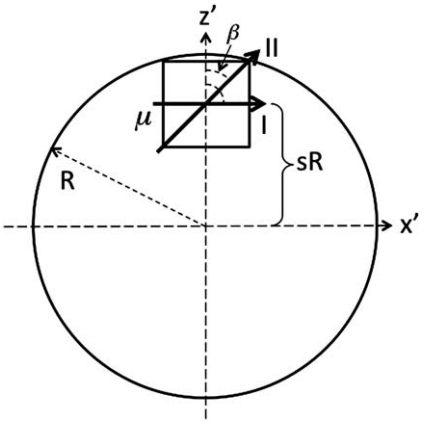

Fig. 1 Two-dimensional illustration of the spherical and magnetic colloid with radius R and with an enclosed magnetic cube with its center localized at $z' = sR$ having a point magnetic moment $\boldsymbol{\mu}$ making the angle $\beta = 90^\circ$ (System I) or $\beta = 45^\circ$ (System II) with respect to the z'-axis of the colloidal (local) coordinate frame.

with respect to the z'-axis. We will consider systems without and with a homogeneous external magnetic field applied.

The total interaction energy U of the system can be expressed as a sum of two terms according to

$$U = U_{\text{part}} + U_{\text{ext}} \tag{1}$$

where U_{part} denotes the interaction energy among the particles and U_{ext} the interaction between the external field and the particles. The former is given as a sum of pair potentials according to

$$U_{\text{part}} = \sum_{i<j} u(\mathbf{r}_{ij}, \boldsymbol{\mu}_i, \boldsymbol{\mu}_j) \tag{2}$$

where $u(\mathbf{r}_{ij}, \boldsymbol{\mu}_i, \boldsymbol{\mu}_j)$ denotes the interaction between particles i and j, and the latter as a single sum

$$U_{\text{ext}} = \sum_i u_{\text{ext}}(\boldsymbol{\mu}_i) \tag{3}$$

where $u_{\text{ext}}(\boldsymbol{\mu}_i)$ denotes the interaction between the external field and particle i. Here, and in the following, $\mathbf{r}_{ij} \equiv \mathbf{r}_i - \mathbf{r}_j$ with $\mathbf{r}_i$ being the location of the center of particle i in an external coordinate frame, whereas $\mathbf{r}_{ij}^{\text{d}} \equiv \mathbf{r}_i^{\text{d}} - \mathbf{r}_j^{\text{d}}$ with $\mathbf{r}_i^{\text{d}}$ being the location of the magnetic dipole of particle i in an external coordinate frame.

Furthermore, the pair interaction energy between particles i and j can be divided into two parts

$$u(\mathbf{r}_{ij}, \boldsymbol{\mu}_i, \boldsymbol{\mu}_j) = u_{\text{HS}}(\mathbf{r}_{ij}) + u_{\text{dd}}(\mathbf{r}_{ij}^{\text{d}}, \boldsymbol{\mu}_i, \boldsymbol{\mu}_j) \tag{4}$$

where the hard-sphere interaction energy $u_{\text{HS}}(\mathbf{r}_{ij})$ is given by

$$u_{\text{HS}}(\mathbf{r}_{ij}) = \begin{cases} \infty, & r_{ij} < 2R \\ 0, & r_{ij} \geq 2R \end{cases} \tag{5}$$

with $r_{ij} \equiv |\mathbf{r}_{ij}|$ and the magnetic dipole–dipole interaction energy $u_{\text{dd}}(\mathbf{r}_{ij}^{\text{d}}, \boldsymbol{\mu}_i, \boldsymbol{\mu}_j)$ by

$$u_{\text{dd}}(\mathbf{r}_{ij}^{\text{d}}, \boldsymbol{\mu}_i, \boldsymbol{\mu}_j) = -\frac{\mu_0}{4\pi}\left[3\frac{(\boldsymbol{\mu}_i \cdot \mathbf{r}_{ij}^{\text{d}})(\boldsymbol{\mu}_j \cdot \mathbf{r}_{ij}^{\text{d}})}{(r_{ij}^{\text{d}})^5} - \frac{\boldsymbol{\mu}_i \cdot \boldsymbol{\mu}_j}{(r_{ij}^{\text{d}})^3}\right] \tag{6}$$

with μ_0 being the permeability in a vacuum and $r_{ij}^{\text{d}} \equiv |\mathbf{r}_{ij}^{\text{d}}|$.

The interaction between the external homogeneous magnetic field $\mathbf{B}_{\text{ext}}$ and the magnetic particle i is given by

$$u_{\text{ext}}(\boldsymbol{\mu}_i) = -\boldsymbol{\mu}_i \cdot \mathbf{B}_{\text{ext}} \tag{7}$$

and, thus, depends on the orientation of the particle with respect to the external field but not on the position of it.

Variables characterizing the fluids of magnetic particles and their values are compiled in Table 1. With the use of dimensionless variables, we get (i) the dimensionless magnetic dipole–dipole interaction energy according to

$$u_{\text{dd}}^*\left(\mathbf{r}_{ij}^{\text{d}*}, \boldsymbol{\mu}_i^*, \boldsymbol{\mu}_j^*\right) = -\left(8\mu_i^*\mu_j^*\right)\left[3\frac{\left(\hat{\boldsymbol{\mu}}_i \cdot \mathbf{r}_{ij}^{\text{d}*}\right)\left(\hat{\boldsymbol{\mu}}_j \cdot \mathbf{r}_{ij}^{\text{d}*}\right)}{\left(r_{ij}^{\text{d}*}\right)^5} - \frac{\hat{\boldsymbol{\mu}}_i \cdot \hat{\boldsymbol{\mu}}_j}{\left(r_{ij}^{\text{d}*}\right)^3}\right] \tag{8}$$

with $\hat{\boldsymbol{\mu}}_i$ denoting the normalized magnetic dipole of particle i and (ii) the dimensionless external interaction energy according to

$$u_{\text{ext}}^*(\boldsymbol{\mu}_i^*) = -\boldsymbol{\mu}_i^* \cdot \mathbf{B}_{\text{ext}}^* \tag{9}$$

The magnetic particle–particle interaction energy and hence the properties of the magnetic fluid will depend on β, denoting the angle between (i) the vector connecting the position of the dipole with the center of the particle and (ii) the direction of the dipole. An analysis of the interaction between two particles in contact (see the Appendix) gives the following: (i) β becomes an irrelevant parameter as $s \to 0$ and (ii) the interaction energy at optimal orientation becomes more negative with increasing β for $s > 0$ at constant μ. Thus, in our case with $s = 0.7$ the interaction energy at optimal orientation of the two particles becomes more negative as β increases from 0° to 90°.

In this work, we will consider two systems differing in their values of β: *viz.* System I with $\beta = 90^\circ$ and System II with $\beta = 45^\circ$. For magnetic particles with $s = 0.7$, the dimensionless magnetic

Table 1 Variables and values characterizing the systems investigated

Variable		Value
Number of particles	N	500
Particle hard-sphere radius	R	
Dimensionless distance	$r^* \equiv r/R$	
Dimensionless particle number density (quasi-2D)	$\rho_{\text{A}}^* \equiv \rho_{\text{A}}(2R)^2$	0.07
Offset of the dipole location	s	0.7[a]
Dipole z'-axis angle	β	45° and 90°
Direction of external field		Along x- and z-axes
Dimensionless magnetic dipole	$\boldsymbol{\mu}^* \equiv X\boldsymbol{\mu}$	4.3, 5.8, 7.2, and 8.6
Dimensionless external field	$\boldsymbol{B}_{\text{ext}}^* \equiv (Xk_{\text{B}}T)^{-1}\boldsymbol{B}_{\text{ext}}$	3.9
Scaling factor	$X \equiv [\mu_0/[(4\pi)k_{\text{B}}T (2R(1-s))^3]]^{1/2}$	
Dimensionless dipole–dipole energy	$u_{\text{dd}}^* \equiv u_{\text{dd}}/(k_{\text{B}}T)$	
Dimensionless external energy	$u_{\text{ext}}^* \equiv u_{\text{ext}}/(k_{\text{B}}T)$	

[a] Taken from the colloids used in the experiments made by Sacanna *et al.*[15]

dipole–dipole interaction energy at optimal particle orientations becomes $u^*_{dd}(\mathbf{r}^{d*}_{ij}, \boldsymbol{\mu}^*_i, \boldsymbol{\mu}^*_j)/(8\mu^*_i\mu^*_j) = -1/8$ for $\beta = 90^\circ$ and -0.0766 for $\beta = 45^\circ$ (again, see the Appendix).

3 Methods

Static properties of the model fluid containing the magnetic particles were determined by means of Monte Carlo (MC) simulations in the NVT ensemble. The particles were confined on a single and quadratic area (quasi-2D space), and periodic boundary conditions in the *xy*-directions were applied. The dipole–dipole interaction is long-ranged, and the Ewald summation with tinfoil boundary conditions was used to improve the handling of the dipole–dipole interaction.[20]

The simulations utilized single-particle trial moves with a maximal translation of $0.5R$ and a maximal rotation of 15° as well as cluster translational trial moves with a maximal translation of $0.5R$. A cluster trial move involves the simultaneous move of a particle and nearby particles. Such a trial move can strongly enhance the sampling of structured systems.[21] Particles possessing center-to-center separation smaller than the predefined cluster radius $r^*_{cutoff} = 2.3$, directly or indirectly, were considered as tentative cluster members. About one percent of the trial moves were cluster trial moves.

The magnetic particles were initially placed randomly, and thereafter they were equilibrated for 1.5×10^6 MC passes (trial moves per particle). Systems with an external field were subsequently equilibrated with the external field applied for another 1.5×10^6 MC passes. The production runs comprised at least 1.5×10^6 MC passes.

Properties of the fluids have been examined by considering:

(1) radial distribution functions $g(r^*)$ providing the local number density normalized by the average number density at the distance r^* from a particle;

(2) angular distribution functions $P[\cos(\psi_{dd})]$ denoting the probability of the cosine of the angle ψ_{dd} formed by the directions of the dipole moments of two particles (Fig. 2);

(3) angular distribution functions $P[\cos(\psi_{rd})]$ denoting the probability of the cosine of the angle ψ_{rd} formed by the particle center-to-center vector and the direction of the dipole moment of either of two particles (Fig. 2);

(4) cluster size distribution functions; and

(5) ensemble-averaged particle–particle and particle–external-field interaction energies.

The two angular distribution functions were averaged over pairs of particles located within the cutoff separation $r^*_{cutoff} = 2.3$, being the same cutoff as for the cluster trial moves.

4 Results

4.1 No external magnetic field

We will start by considering final configurations for the magnetic dipole moments $\mu^* = 4.3$ and 8.6 without an external field for Systems I and II. Fig. 3 shows that the tendency of dimer formation is low at $\mu^* = 4.3$ (Fig. 3a and b), whereas at $\mu^* = 8.6$ essentially all colloids appear in clusters containing two to four colloids (Fig. 3c and d). The tendency of cluster formation appears to be similar in Systems I and II; however, cluster size distribution functions (data not shown) show that the cluster formation is somewhat stronger in System I.

The structure of the fluids has been investigated by radial distribution functions. In Fig. 4a and b, we focus on $g(r^*)$ near the contact separation $r^* = 2$. For $\mu^* = 4.3$ and 5.8, we notice that the local density at the separation, at which two colloids are in hard-sphere contact ($r^* = 2$), is larger in System I than in System II. Nevertheless, at the two largest values of μ^* the local densities at $r^* = 2$ are similar to the two systems.

The results of the dipole–dipole angular analysis are presented in Fig. 4c and d. In general, we find an enhanced

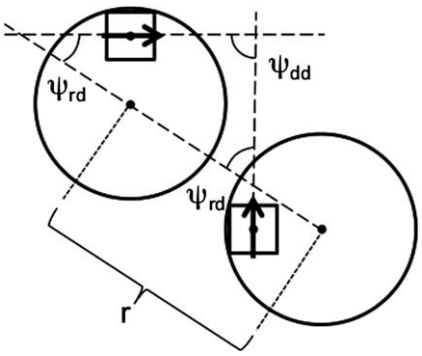

Fig. 2 Two-dimensional illustration of two neighboring colloids at the center-to-center separation r with the dipole–dipole angle ψ_{dd} and the center-to-center-dipole angle ψ_{rd} defined.

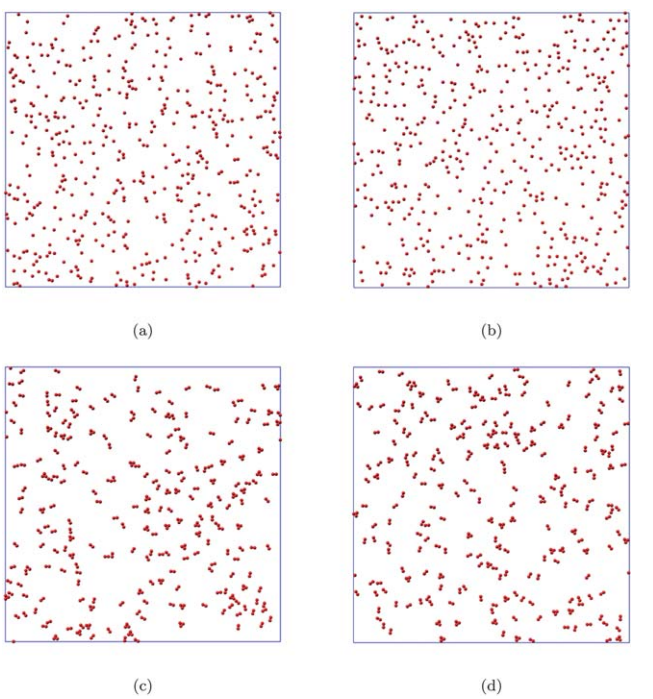

Fig. 3 Snapshots of fluids of spherical colloids possessing the dimensionless magnetic moment (a and b) $\mu^* = 4.3$ and (c and d) $\mu^* = 8.6$ of (a and c) System I and (b and d) System II.

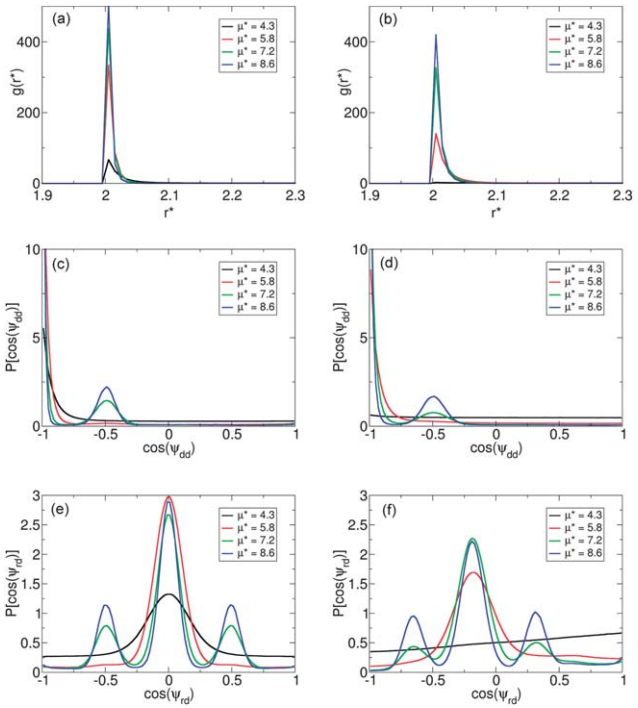

Fig. 4 (a and b) Radial distribution function $g(r^*)$, (c and d) angular distribution function $P[\cos(\psi_{dd})]$, and (e and f) angular distribution function $P[\cos(\psi_{rd})]$ for (a, c, and e) System I and (b, d, and f) System II at indicated values of the dimensionless magnetic moment.

probability for $\cos(\psi_{dd}) \approx -1$, representing an anti-parallel orientation of the dipoles of neighboring colloids. At the two larger values of μ^*, an enhanced probability also appears for $\cos(\psi_{dd}) \approx -0.5$, corresponding to $\psi_{dd} \approx 120^\circ$. In particular, we notice in System I as compared to System II (i) for $\mu^* = 4.3$ a much stronger correlation of the dipolar directions for neighboring colloids and (ii) for $\mu^* = 7.2$ a larger probability for $\psi_{dd} \approx 120^\circ$ is achieved, signaling triangular clusters of trimers.

The angular distribution function between the dipole moment and the directional vector $\mathbf{r}_{ij}$ shown in Fig. 4e and f gives further information on the orientation of the dipoles of neighboring colloids. First, in System I, but not in System II, $P[\cos(\psi_{rd})]$ possesses an even symmetry about $\cos(\psi_{rd}) = 0$. That is of course related to the fact that the dipole vector is perpendicular to the z'-axis, *i.e.*, $\beta = 90^\circ$, in System I (see Fig. 1). We find an enhanced probability for $|\cos(\psi_{dd})| \approx 0.5$, *i.e.*, $\psi_{dd} \approx 60^\circ$ and 120° representing a dipole directed perpendicular to the bisector of the angle formed by three triangularly positioned particles. Again, in System I as compared to System II (i) for $\mu^* = 4.3$ a much stronger correlation of the dipolar direction with respect to the colloid–colloid vector and (ii) for $\mu^* = 7.2$ a larger fraction of the triangular arrangement, signaling triangular clusters of trimers, are found.

The two angular distribution functions jointly give a clear view of angular correlations appearing in dimers and trimers formed. In System I, the colloids align such that their dipoles are anti-parallel, which is the most favorable configuration that two of these dipoles can form. In contrast, the alignment of the colloids in System II is less favorable by the requirement of a *longer* dipole–dipole separation for a perfect anti-parallel arrangement. As shown in the Appendix, (i) the absolute value of the attractive energy minimum increases with increasing value of β, (ii) at $s = 0.7$ energy minima are obtained for a perfect anti-parallel orientation for all values of β, and (iii) in particular, the ratio of the attractive energy minima of System I ($\beta = 90^\circ$) to System II ($\beta = 45^\circ$) is $(1/8)/0.0766 = 1.63$.

Ensemble averages of the dipole–dipole interaction energy and dipole–external field interaction energy, both per particle and k_BT, are provided in Table 2. First, $|\langle U^*_{part}\rangle| \gg 1$ except for $\mu^* = 4.3$ in System II where $|\langle U^*_{part}\rangle| < 1$. Here, the dipole–dipole interaction energy is too weak to induce a significant orientational ordering as supported by Fig. 4d and f. Second, we find that the averaged dipole interaction energy is more negative in System I as compared to System II. At $\mu^* = 8.6$ and 7.2, the ratio $\langle U^*_{part}\rangle_{System\ I}/\langle U^*_{part}\rangle_{System\ II}$ becomes 1.66 and 1.73, which is essentially equal to 1.63. This finding supports the interaction analysis in the Appendix and is consistent with the strong ordering shown in Fig. 4c–f at $\mu^* = 8.6$ and 7.2. Third, at $\mu^* \geq 5.8$ for System I and at $\mu^* \geq 7.2$ for System II, we have $\langle U^*_{part}\rangle \propto (\mu^*)^2$. Taken together, the two last observations are consistent with a basically equal structure among the five systems specified by $\mu^* \geq 5.8$ for System I and $\mu^* \geq 7.2$ for System II.

Table 2 Ensemble-averaged and dimensionless particle–particle $\langle U^*_{part}\rangle$ and particle–external-field $\langle U^*_{ext}\rangle$ interaction energy of the different systems studied[a]

		No field	Parallel field			Perpendicular field		
System	μ^*	$\langle U^*_{part}\rangle$	$\langle U^*_{part}\rangle$	$\langle U^*_{ext}\rangle$	$\langle U^*_{part}\rangle/\langle U^*_{ext}\rangle$	$\langle U^*_{part}\rangle$	$\langle U^*_{ext}\rangle$	$\langle U^*_{part}\rangle/\langle U^*_{ext}\rangle$
I	4.3	−4.53	−0.21	−15.79	0.01	0.17	−16.10	−0.01
I	5.8	−29.14	−7.42	−21.94	0.34	−0.41	−21.72	0.02
I	7.2	−48.98	−34.36	−28.05	1.23	−12.69	−26.28	0.48
I	8.6	−72.84	−50.64	−33.30	1.52	−38.32	−24.11	1.59
II	4.3	−0.13	−0.14	−16.13	0.01	0.18	−16.11	−0.01
II	5.8	−10.17	−0.38	−22.83	0.02	0.31	−21.81	−0.01
II	7.2	−28.32	−6.40	−28.48	0.23	0.45	−27.52	−0.02
II	8.6	−43.91	−35.23	−32.09	1.10	0.56	−33.20	−0.02

[a] $\langle U^*_{part}\rangle \equiv \langle U_{part}\rangle/(Nk_BT)$ and $\langle U^*_{ext}\rangle \equiv \langle U_{exit}\rangle/(Nk_BT)$ with U_{part} given by eqn (2) and U_{ext} given by eqn (3), and where $\langle\ldots\rangle$ denotes a canonical ensemble average.

In summary, the colloids with a single magnetic dipole located at $s = 0.7$ (i) remain as monomers at low values of the magnetic dipole moment; (ii) form dimers at larger values of the dipole moment; (iii) form triangular trimers at even larger values of the dipole moment; (iv) do not form elongated structures; and (v) for a constant value of the dipole moment the colloid cluster formation is strongest when the angle between the direction of the off-center dipole and of its local radial vector is perpendicular, *i.e.*, $\beta = 90°$. Issue (iv) contrasts to the observed formation of a linear chain of colloids with a central dipole ($s = 0$) at sufficiently large magnitude of the magnetic moment.

4.2 External magnetic field

The effect of an external magnetic field on the quasi-2D systems differs strongly between the field applied parallel (x-direction) and perpendicular (z-direction) to the plane of the colloids.

4.2.1 Parallel magnetic field. Final configurations of systems with the largest magnetic moment $\mu^* = 8.6$ for Systems I and II with an external field parallel to the plane of the colloids are given in Fig. 5. At these conditions, practically all colloids form extended (infinite) chains. The final configurations for $\mu^* \leq 5.8$ display that no chain formation appears (configurations not shown) at these conditions.

The corresponding radial distribution functions for all values of μ^* are given in Fig. 6a and b; now with the abscissa extended up to $r^* = 8$. For the smallest magnetic dipole moment only a very small tendency of dimer formation is present, in fact the probability for dimers in System I is *lowered* as compared to no field applied [the value of $g(r^* = 2)$ is reduced from 15 to 1.9 by applying the field]. With increasing dipole moment the frequency of two colloids to being in close contact increases and subsequently maxima at $r^* \approx 3.6, 4.1, 5.5, 6.2, \ldots$ appear. Again, the structuring starts to appear at smaller values of μ^* for System I as compared to System II. Furthermore and noticeably, the maxima do *not* appear at $r^* = 2n$, n integer; hence, we do not have chains of linearly arranged colloids. In fact, the colloids are arranged in a zigzag pattern (as latter illustrated).

The dipole–dipole angular distribution functions shown in Fig. 6c and d now display a large probability for $\cos(\psi_{dd}) \approx 1$, *i.e.*, *parallel* orientation of the dipoles of neighboring colloids. Except for the largest $\mu^* = 8.6$ for System II, the maxima at $\cos(\psi_{dd}) = 1$ is the only maximum of the angular distributions. Obviously, by applying a sufficiently strong external field the structure appearing without a field, as described in Section 4.1, is broken down and a new structure is formed.

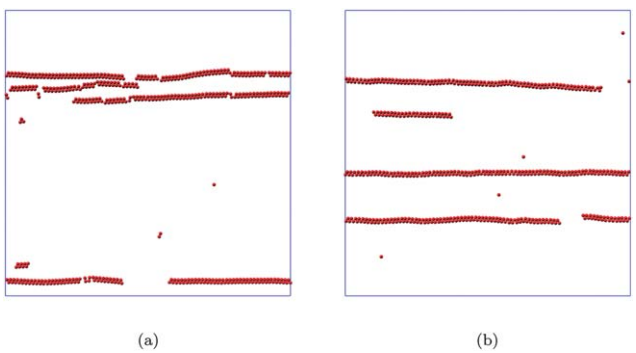

Fig. 5 Snapshots of fluids of spherical colloids possessing the dimensionless magnetic moment $\mu^* = 8.6$ with an external magnetic field in the x-direction for (a) System I and (b) System II.

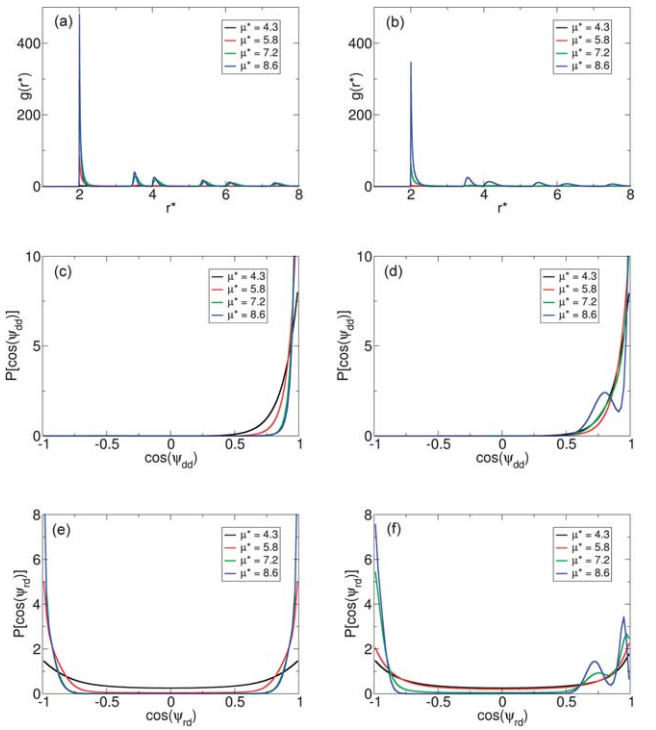

Fig. 6 (a and b) Radial distribution function $g(r^*)$, (c and d) angular distribution function $P[\cos(\psi_{dd})]$, and (e and f) angular distribution function $P[\cos(\psi_{rd})]$ for (a, c, and e) System I and (b, d, and f) System II with an external magnetic field in the x-direction at indicated values of the dimensionless magnetic moment.

The angular distribution functions between the dipole moment and the directional vector $\mathbf{r}_{ij}$ in Fig. 6e and f display in most cases clear maxima at $|\cos(\psi_{dd})| = 1$, implying that the magnetic dipoles of neighboring colloids are oriented head-to-tail. As without a field, System I displays (i) inversion symmetry about $\cos(\psi_{rd}) = 0$ and (ii) a greater probability of ordering as compared to System II.

As stated earlier, in System II an optimal orientation of the directions of neighboring dipoles is achieved by an increasing distance between the dipoles, making the dipole–dipole interaction weaker and the angular orientation less prominent.

As to the energetic analysis, from the data in Table 2 we extract that (i) $|\langle U^*_{ext}\rangle| \gg 1$, *i.e.*, larger than the thermal energy and (ii) $\langle U^*_{ext}\rangle \approx -\mu^* B^*$ in all cases showing that the dipoles are oriented parallel to the external magnetic field. Furthermore, when applying the parallel magnetic field the value of $|\langle U_{part}{}^*\rangle|$ is reduced, *i.e.*, showing a less favorable dipole–dipole interaction, consistent with changes of the two types of angular distribution functions upon applying the external field (*cf.* Fig. 6c–f with Fig. 4c–f). The only exception is for $\mu^* = 4.3$ in System II, where we also find $|\langle U^*_{part}\rangle| < 1$, also for the case of no external field, implying no significant dipolar order.

4.2.2 Perpendicular magnetic field. Configurations for systems with the largest magnetic moment $\mu^* = 8.6$ with an external field perpendicular to the plane of the colloids are shown in Fig. 7. In contrast to a parallel magnetic field, *no* chain formation appears with a perpendicular field. In fact, System I appears to have a similar cluster structure as with no field (*cf.* Fig. 7a with Fig. 3c), whereas the dimerization in System II is weakened (*cf.* Fig. 7b with Fig. 3d).

A comparison of the radial distribution functions obtained with an external field perpendicular to the plane given in Fig. 8a and b with those obtained with no field applied given in Fig. 4a and b shows that the external field *reduces* the local density of other colloids near a colloid. In particular, Fig. 8b shows that in System II colloids are depleted from the nearest vicinity of a colloid signaling that the colloids are *repelling* each other. Furthermore, we notice that the repulsion increases with increasing magnetic dipole moment.

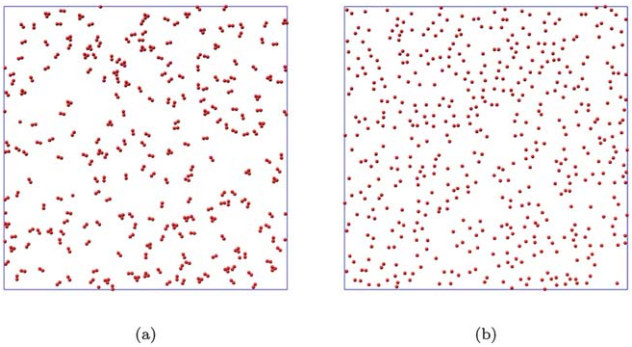

Fig. 7 Snapshots of fluids of spherical colloids possessing the dimensionless magnetic moment $\mu^* = 8.6$ with an external magnetic field in the z-direction for (a) System I and (b) System II.

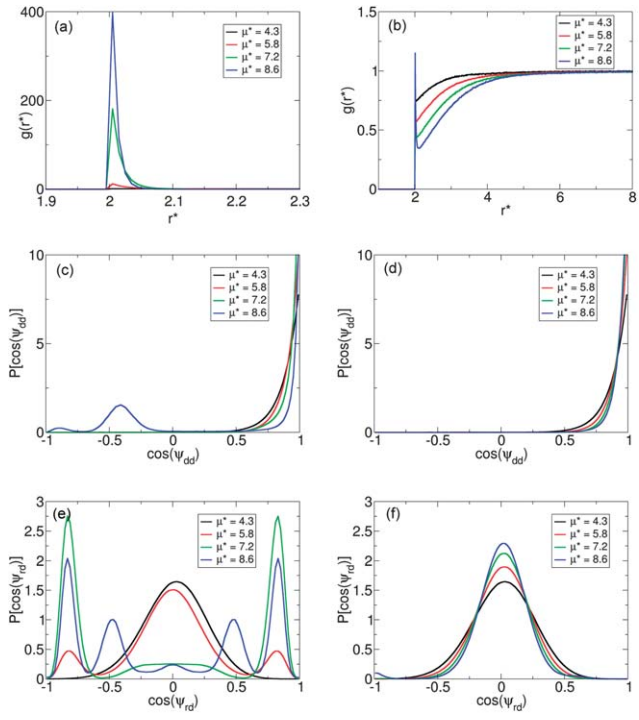

Fig. 8 (a and b) Radial distribution function $g(r^*)$, (c and d) angular distribution function $P[\cos(\psi_{dd})]$, and (e and f) angular distribution function $P[\cos(\psi_{rd})]$ for (a, c, and e) System I and (b, d, and f) System II with an external magnetic field in the z-direction at indicated values of the dimensionless magnetic moment.

The dipole–dipole angular distribution functions displayed in Fig. 8c and d again show a preference for a parallel arrangement of the directions of the dipole moments in neighboring colloids. Only for System I with the largest magnetic moment $\mu^* = 8.6$ an additional maximum at $\cos(\psi_{dd}) \approx -0.4$ occurs, implying the presence of some trimers in a triangular arrangement.

Finally, angular distribution functions between the dipole moment and the directional vector $\mathbf{r}_{ij}$ are given in Fig. 8e and f. In System II, this distribution now essentially becomes inversion symmetric and the direction of the dipoles is perpendicular to the colloid–colloid vector and hence *parallel* to the external field, albeit with a broad distribution. Hence, we conclude that the dipoles are arranged side-by-side rather than head-to-tail as for the case of a parallel external field. In System I, the situation is more complicated. For the smallest magnetic moment $\mu^* = 4.3$, the direction of the dipoles adheres to that in System II. With increasing magnetic moment the probability of the magnetic moment to be oriented in the field is *reduced* and the probability of head-to-tail-like arrangements is increased. However, the external field gives rise to a net orientation of the dipoles in the field direction and prohibits perfect head-to-tail configurations, as evident from the maxima appearing at $|\cos(\psi_{dd})| \approx 0.8$ in Fig. 8e instead of at $|\cos(\psi_{rd})| = 1$ for a perfect alignment. We obviously discern the competition between the dipole–field interaction dominating at low dipole magnitude favoring a parallel dipole orientation and dipole–dipole interaction dominating at high dipole magnitude favoring a triangular dipole configuration.

Also with an external perpendicular magnetic field, we first observe (i) $|\langle U^*_{ext}\rangle| \gg 1$ in all cases and (ii) $\langle U^*_{ext}\rangle \approx -\mu^* B^*$ in all cases except one, again showing that the dipoles are oriented predominantly parallel to the external magnetic field. The exception appears for System I with $\mu^* = 8.6$. Observation (ii) cannot hold at sufficiently large μ^* for a given B^*, since the dipole–dipole interaction energy depends on $(\mu^*)^2$ and the dipole–external field interaction energy on μ^*. The reason that finding (ii) breaks down earlier with a perpendicular field as compared to a parallel field is that the external field more strongly perturbs the structure in the former case. Second, $|\langle U^*_{part}\rangle|$ is close to zero in all cases except just for System I with $\mu^* = 8.6$ and also to some extent for System I with $\mu^* = 7.2$. For System I with $\mu^* = 7.2$ and 8.6, Fig. 8e shows a prominent probability of a head-to-tail orientation. Such an orientation was completely absent for System II (as shown by Fig. 8d), in agreement with the observations $\langle U^*_{part}\rangle \approx +0.5$ in these cases.

5 Discussion

The aim of our investigation was to find a model system displaying similarities to those found by Sacanna *et al.*[15] in their study of solutions of colloidal particles with an off-centered

magnetic hematite cube in quasi-2D space and possibly clarify some experimental questions. In the following, we will first discuss our model results of colloidal particles in the quasi-2D space. Thereafter, these results will be compared with the corresponding experimental findings.

5.1 Model results

System I with $\beta = 90^\circ$ and System II with $\beta = 45^\circ$ display qualitatively the same behavior, including that with an external magnetic field present, though a higher magnetic moment was required in System II to achieve the same or a similar structure as that in System I. As alluded to in the Method section and analyzed in the Appendix, our model system of magnetic dipoles having a large (but fixed) off-centered location displays the largest tendency of forming structures when the angle between the dipole and the radial vector of the dipole is $\beta = 90^\circ$ and the smallest tendency for $\beta = 0^\circ$.

For small values of s, the structure formed by two neighboring particles involves a dipolar head-to-tail alignment, whereas for large values of s the side-by-side anti-parallel alignment becomes the preferred one. For $\beta = 0^\circ$, the transition zone between head-to-tail and side-by-side antiparallel arrangements ranges from $s' \approx 0.4$ to $s'' \approx 0.6$ as analyzed by Kantorovich[16] and also shown in the Appendix. When $\beta > 0^\circ$, the transition starts already at $s' = 0_+$ and ends at s'' with s'' reducing from 0.6 to 0.4 as β increases from 0° to 90°.

In Fig. 9, we summarize graphically some key results taken from Systems I and II. In the absence of an external magnetic field, colloidal dimers are dominating at intermediate magnetic moment, see Fig. 9a. The colloids are oriented such that the dipoles face each other, and the dipole–dipole distance becomes larger in System II. At a larger magnetic moment, clusters of three colloids are formed, oriented such that their dipoles face the joint mass center of the colloids, see Fig. 9b.

In the presence of an external homogeneous magnetic field, the direction of the field has a pronounced influence on the structure. With the field parallel to the plane of the colloids, long chains of colloids arranged in a zigzag pattern was obtained, as seen in Fig. 9c, with the colloids oriented such that the dipoles are close to the central line of the chain. Here, the external field aligns in the directions of the dipoles (i) parallel to the plane of the colloids and (ii) in the direction of the field, both facilitating a head-to-tail like dipole–dipole arrangement. Finally, by applying an external field perpendicular to the plane of the colloids of a sufficient strength as compared to the colloidal dipole–dipole interaction, any existing dimers and trimers are disintegrated as illustrated in Fig. 9d. The field affects the directions of the dipoles to become more perpendicular to the plane of the colloids, and with such an ordering, the dipoles of the colloids (forced to be in one plane) become parallel and hence are repelling each other.

In summary, System I and System II display similar structures, but the ability to form stronger dipole–dipole interactions in System I makes the structures more developed in System I as compared to System II for the same magnetic moment.

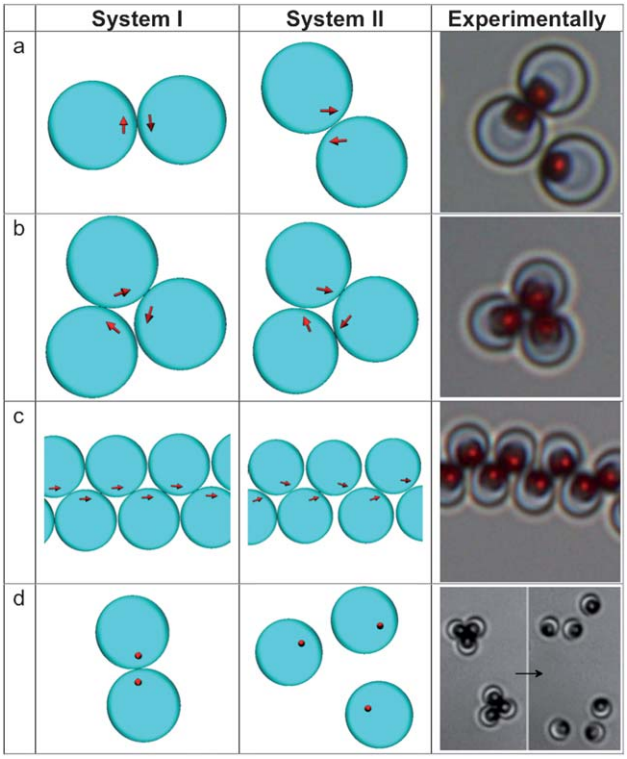

Fig. 9 Comparison of current model predictions and experimental findings[15] for (a) dimer formation typically appearing at intermediate magnetic interaction, (b) trimer formation appearing at strong magnetic interaction, (c) chain formation in the presence of a parallel magnetic field, and (d) dimer resistance (System I) and breakup of trimers (System II) in the presence of a perpendicular magnetic field.

5.2 Comparison with experimental data

In the right column of Fig. 9, we reproduce previous results of Sacanna *et al.*[15] for the same conditions. We indeed satisfactorily find a qualitative agreement between the properties of our model system and the findings by Sacanna *et al.* for all cases. The convincing agreement thus suggests that the colloidal spheres with an off-centered hematite cube can, at least initially, be represented by hard spheres with a single off-center magnetic dipole moment. In particular, we notice that the agreeing zigzag structure shown in Fig. 9c strongly supports the notion that the appearance of such a structure is due to the off-centered location of the magnetic material in the colloids.

It should be noted that we have employed a single value of the off-centered factor $s = 0.7$, determined from visual inspection of images such as those given in Fig. 9. Given that value, our study provides an insight into the magnitude of the magnetic moments necessary for the formation of the different structures observed. Furthermore, we notice that the experimental colloids are charged; however, the concentration of simple salt is high enough to screen the electrostatic repulsion making it very short-range as compared to the colloidal size and the range of the magnetic dipole–dipole interaction. In fact, Sacanna *et al.*[15] showed that colloidal cluster formation was suppressed at lower concentration of simple salt.

We end by making some tentative conclusions on the experimental systems based on a comparison of the still limited experimental imaging data and the model results:

(i) For a given strength of the magnetic field, we have established a lower limit of the magnetic moment of the colloids for obtaining a linear ordered structure. As this lower limit depends on the angle β, a possible route is to use experimental values of the magnetic moment and the external field and assess the value of β by fitting experimental results.

(ii) In a linearly ordered structure, the magnetic cube of one colloid is not located symmetrically with respect to the two neighbors. Specifically, pairs of magnetic cubes are observed (Fig. 9c) suggesting that if colloids with $\beta = \beta'$ are present, also colloids with $\beta = 180^\circ - \beta'$ are present, *e.g.*, by the hematite cubes incorporated into the spheres in different directions still having one side oriented essentially parallel to the nearby colloidal surface. This observation obviously indicates that in the experimental setup $\beta \neq 90^\circ$.

More experimental data enabling better statistical averages and simulations of systems with a mixture of colloids possessing $\beta = \beta'$ and $\beta = 180^\circ - \beta'$ for different values of β' are most likely need to make further progress to assign the direction(s) of the magnetic moment of the hematite cubes with respect to the radial axis of the colloids.

6 Conclusion

Though its simplicity, a number of features of the coarse-grained model agree with recent experimental observations, supporting the applicability of the model. Specific properties of fluids of magnetic colloids with an off-centered magnetic region such as (i) a suppressed probability of forming linear chains, (ii) an antiparallel dipole–dipole alignment of nearby dipoles, and (iii) the formation of linear zigzag chains in the presence of an external field are reproduced. Furthermore, we observed an increase of strength of the dipole–dipole interaction with increasing angle between the dipole direction and the vector joining the center of the particle and the location of the dipole.

The simulation technique offers possibilities to examine features yet difficult to access experimentally. Obvious extensions of the model system to further mimic experimental systems include (i) properties of fluids of magnetic colloids containing a mixture of colloids with different internal structures such as a variation of the direction of the dipole and/or the radial location of the dipole – the mixture mimicking either a natural polydispersity or polydispersity prepared from different batches of magnetic colloids and (ii) particles with several magnetic regions.

Finally, colloids with more than one magnetic domain will broaden the scope even more for designing colloidal structure mimicking the formation of molecules by atoms. Colloids with two, three, or four magnetic domains mutually separated and near the colloid surface would resemble the sp, sp^2 and sp^3 hybridization of a carbon and the colloid with one domain would resemble a hydrogen in hydrocarbon molecules. An increased ability to fabricate magnetic particles with several magnetic domains in controlled positions will enable a multitude of possibilities to realize reversible formation of various colloidal structures.

7 Appendix: interaction energy between two hard spheres with embedded off-centered dipoles

In the appendix we consider the dipole–dipole interaction energy between two hard spheres with off-centered dipoles. The results provided here will rationalize observations described in the main part of the paper.

As illustrated in Fig. 10, we consider two hard spheres with radius R at contact. In the external Cartesian xyz-coordinate frame, both spheres are located on the z-axis with sphere i at $z_i = R$ and j at $z_j = -R$. A local Cartesian $x'y'z'$-coordinate frame is associated with each sphere. The origin of the $x'y'z'$-coordinate frame is positioned at the center of the sphere and is rotated α radians about the y'-axis. Furthermore, a dipole $\boldsymbol{\mu}$ is embedded in each sphere (i) on the z'-axis displaced sR from the origin, and (i) rotated β radians about the y'-axis. The vector $\mathbf{r}^d$ denotes the location of a dipole in the external coordinate frame.

We will now express the dipole–dipole interaction energy between the two dipoles as a function of s and the angles β, α_i, and α_j. To do so, the dipole moments and their locations are preferably expressed in the external coordinate frame according to

$$\boldsymbol{\mu}_i = \mu[\sin(\alpha_i + \beta), 0, \cos(\alpha_i + \beta)] \quad (10)$$

$$\boldsymbol{\mu}_j = \mu[\sin(\alpha_j + \beta), 0, \cos(\alpha_j + \beta)] \quad (11)$$

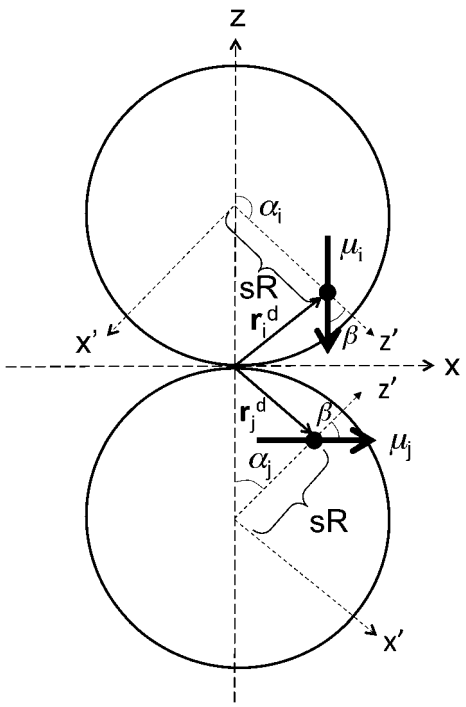

Fig. 10 Two-dimensional illustration of two hard spheres with embedded magnetic dipole at contact. All symbols are defined in the text.

$$\mathbf{r}_i^{\mathrm{d}} = R[s\,\sin(\alpha_i),\ 0,\ 1 + s\,\cos(\alpha_i)] \tag{12}$$

$$\mathbf{r}_j^{\mathrm{d}} = R[s\,\sin(\alpha_j),\ 0,\ -1 + s\,\cos(\alpha_j)] \tag{13}$$

and the vector joining the two dipoles becomes

$$\mathbf{r}_{ij}^{\mathrm{d}} \equiv \mathbf{r}_i^{\mathrm{d}} - \mathbf{r}_j^{\mathrm{d}} = R[s(\sin(\alpha_i) - \sin(\alpha_j)),\ 0,\ 2 + s(\cos(\alpha_i) - \cos(\alpha_j))] \tag{14}$$

In the following, the *scaled* dipole–dipole interaction energy given by

$$\begin{aligned} u^{\mathrm{scaled}}\left(\mathbf{r}_{ij}^{\mathrm{d}*}, \boldsymbol{\mu}_i^*, \boldsymbol{\mu}_j^*\right) &\equiv \frac{u_{\mathrm{dd}}^*\left(\mathbf{r}_{ij}^{\mathrm{d}*}, \boldsymbol{\mu}_i^*, \boldsymbol{\mu}_j^*\right)}{8\mu_i^*\mu_j^*} \\ &= -\frac{1}{\left(r_{ij}^{\mathrm{d}*}\right)^5}\left[3\left(\hat{\boldsymbol{\mu}}_i\cdot\mathbf{r}_{ij}^{\mathrm{d}*}\right)\left(\hat{\boldsymbol{\mu}}_j\cdot\mathbf{r}_{ij}^{\mathrm{d}*}\right) - \left(\hat{\boldsymbol{\mu}}_i\cdot\hat{\boldsymbol{\mu}}_j\right)\left(\mathbf{r}_{ij}^{\mathrm{d}*}\cdot\mathbf{r}_{ij}^{\mathrm{d}*}\right)\right] \end{aligned} \tag{15}$$

will be used. We notice that $u^{\mathrm{scaled}}(\mathbf{r}_{ij}^{\mathrm{d}*}, \boldsymbol{\mu}_i^*, \boldsymbol{\mu}_j^*)$ depends on s and the angles β, α_i, and α_j through eqn (10)–(14). The full expression of $u^{\mathrm{scaled}}(s, \beta, \alpha_i, \alpha_j)$ is lengthy, but for $\beta = 0$ it reduces to

$$\begin{aligned} u^{\mathrm{scaled}}(s,\ 0,\ \alpha_i,\ \alpha_j) = \frac{1}{\left(r_{ij}^{\mathrm{d}*}\right)^5} &\times \left\{s^2\left[\left(1-\cos\left(\alpha_i-\alpha_j\right)\right)\left(3-\cos\left(\alpha_i-\alpha_j\right)\right)\right]\right. \\ &+ 2s\left[\left(\cos(\alpha_i)-\cos\left(\alpha_j\right)\right)\left(3-\cos\left(\alpha_i-\alpha_j\right)\right)\right] \\ &\left.+ 4\left[\cos\left(\alpha_i-\alpha_j\right) - 3\cos(\alpha_i)\cos\left(\alpha_j\right)\right]\right\} \end{aligned} \tag{16}$$

and for $\beta = \pi/2$ to

$$\begin{aligned} u^{\mathrm{scaled}}(s,\ \pi/2,\ \alpha_i,\ \alpha_j) = \frac{1}{\left(r_{ij}^{\mathrm{d}*}\right)^5} &\left\{s^2\left[2\,\cos\left(\alpha_i-\alpha_j\right)\right.\right. \\ &\times\left[1-\cos\left(\alpha_i-\alpha_j\right)\right] - 3\,\sin^2\left(\alpha_i-\alpha_j\right)\Big] \\ &+ 2s\left[2\,\cos\left(\alpha_i-\alpha_j\right)\left(\cos(\alpha_i)-\cos\left(\alpha_j\right)\right)\right. \\ &\left.+ 3\,\sin\left(\alpha_i-\alpha_j\right)\left(\sin(\alpha_i)+\sin\left(\alpha_j\right)\right)\right] \\ &\left.+ 4\left[\cos\left(\alpha_i-\alpha_j\right) - 3\,\sin(\alpha_i)\sin\left(\alpha_j\right)\right]\right\} \end{aligned} \tag{17}$$

with

$$r_{ij}^{\mathrm{d}*} = \{2s^2[1 - \cos(\alpha_i - \alpha_j)] + 4s(\cos(\alpha_i) - \cos(\alpha_j)) + 4\}^{1/2} \tag{18}$$

The scaled dipole–dipole interaction energy $u^{\mathrm{scaled}}(s, \beta, \alpha_i, \alpha_j)$ given by eqn (10)–(15) was numerically minimized with respect to α_i and α_j for $0 \le s < 1$ and $0 \le \beta/\pi \le 1/2$ using Powell's method.[22] For $\beta = 0$ our results agree with those of Kantorovich *et al.*[16] In the following, the angles α_i and α_j, denoting the orientation of the hard spheres in the external coordinate frame, will be replaced by $\gamma_i \equiv \alpha_i + \beta$ and $\gamma_j \equiv \alpha_j + \beta$, denoting the orientation of the magnetic dipoles in the external coordinate frame.

The values of the angles γ_i and γ_j in the range $[-\pi, \pi]$ and their difference $\gamma_i - \gamma_j$ as a function of s at various values of β at minimized interaction energy are given in Fig. 11.

(1) For $\beta = 0$, there is a regime extending from $s = 0$ (central dipoles) to $s = s'$ with $s' \approx 0.4$, for which the dipoles remain head-to-tail aligned ($\gamma_i = \gamma_j = 0$). In the regime with large s, $s > s''$ with $s'' \approx 0.6$, both γ_i and γ_j are nonzero and their difference becomes $(\gamma_i - \gamma_j)/\pi = 1$. Thus, the dipoles are here strictly anti-parallel aligned, and according to Fig. 11a the direction of the dipoles with respect to the external coordinate frame is weakly dependent on s. In the intermediate regime $s' < s < s''$, the angles γ_i and γ_j depend more strongly on s.

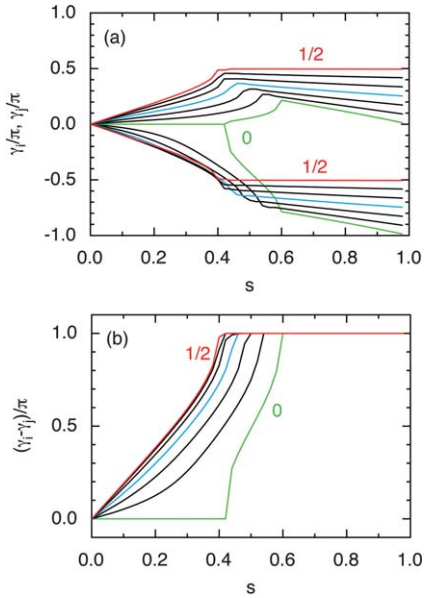

Fig. 11 (a) Angles γ_i and γ_j in the range $[-\pi, \pi]$ and (b) their difference $\gamma_i - \gamma_j$ as a function of s at $\beta/\pi = 0$ (green), 1/12 (black), 1/6 (black), 1/4 (blue), 1/3 (black), 5/12 (black), and 1/2 (red) for the dipole–dipole interaction energy given by eqn (10)–(15) and minimized with respect to α_i and α_j.

(2) For $\beta > 0$, the regime with perfect head-to-tail alignment has formally reduced to $s = 0$ only, and the gradual rotation as represented by γ_i and γ_j with increasing s toward an anti-parallel alignment starts already at $s = 0_+$. The regime with an anti-parallel alignment starts at smaller s as β is increased, and at $\beta/\pi = 1/2$ it starts at $s'' = 0.4$. For $\beta/\pi = 1/2$ and $s > s'$, Fig. 11a shows that the dipoles are oriented perpendicular to the z-axis, *i.e.*, perpendicular to the sphere-to-sphere vector.

The related dipole–dipole interaction energy minimized with respect to α_i and α_j as a function of s at various values of β is given in Fig. 12. Two different expressions of the interaction energy will be considered:

(1) Fig. 12a displays $u_{\mathrm{min}}^{\mathrm{scaled}}$ where u^{scaled} is (i) given by eqn (15) and (ii) minimized with respect to α_i and α_j. Hence, the energy dependence of s through $\mathbf{r}_{ij}$ is suppressed, and the energy dependence of s is only through the values of α_i and α_j. Thus, $u_{\mathrm{min}}^{\mathrm{scaled}}$ *vs.* s expresses how the interaction energy responds from a variation of s through the dipolar orientations *only*. With increasing value of s, the attenuation of the attractive dipole–dipole interaction energy is strongest for $\beta = 0$ and weakest for $\beta/\pi = 1/2$. The reason for the different attenuation is that a perfect anti-parallel alignment can be established at *smaller* dipole–dipole separation as β/π is increased from 0 to 1/2. At $\beta/\pi = 1/2$ the attractive dipole–dipole interaction energy is reduced by a factor 2, consistent with the ratio of the dipole–dipole interaction energy for head-to-tail and anti-parallel alignment at the same dipole–dipole separation. For $s'' > 0.4$,

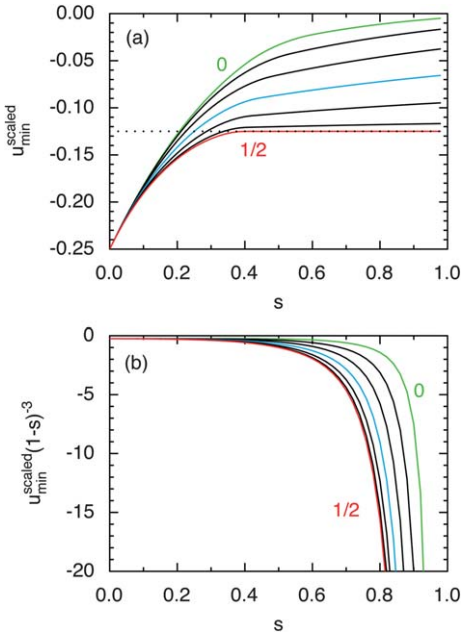

Fig. 12 (a) Minimized scaled dipole–dipole interaction energy $u_{\min}^{\text{scaled}}$ and (b) modified minimized scaled dipole–dipole interaction energy $u_{\min}^{\text{scaled}}(1-s)^{-3}$ ($\propto u_{\text{dd,min}}$) as a function of s at $\beta/\pi = 0$ (green), 1/12 (black), 1/6 (black), 1/4 (blue), 1/3 (black), 5/12 (black), and 1/2 (red) for the dipole–dipole interaction energy given by eqn (10)–(15) and minimized with respect to α_i and α_j.

the constant value of $u_{\min}^{\text{scaled}}$ at $\beta/\pi = 1/2$ is consistent with the constant value of $\gamma_i - \gamma_j$ shown in Fig. 11b.

(2) Fig. 12b shows $(1-s)^{-3}u_{\min}^{\text{scaled}}$, which is proportional to $u_{\text{dd,min}}$ with u_{dd} given by eqn (6). We observe that the dipole–dipole interaction energy minimized with respect to the dipolar orientations is (i) negative (attractive) and (ii) becomes more attractive with increasing s, an effect that originates from the fact that two dipoles, each residing in a colloid, are able to come nearer each other when the dipoles are located closer to the surfaces of the colloids. Earlier, we concluded from Fig. 12a that the dependency on s through the dipolar orientation only attenuates the attractive dipole–dipole interaction.

Thus, as the dipoles are displaced closer to the surfaces of the hard-sphere particles, the dipole–dipole interaction energy of two particles becomes more negative due to shorter dipole–dipole separation, but that increase in magnitude of the interaction is weakly counteracted by a less favorable dipole–dipole orientation.

Acknowledgements

This work was financed by the Swedish Research Council (VR) through the Linnaeus center of excellence Organizing Molecular Matter (Grant no. 239-2009-6794).

References

1 S. Sacanna and D. J. Pine, *Curr. Opin. Colloid Interface Sci.*, 2011, **16**, 96–105.
2 T. D. Nguyen, E. Jankowski and S. C. Glotzer, *ACS Nano*, 2011, **5**, 8892–8903.
3 S. C. Glotzer and M. J. Solomon, *Nat. Mater.*, 2007, **6**, 557–562.
4 J. A. Fan, W. Chihhui, K. Bao, J. Bao, R. Bardhan, N. J. Halas, V. N. Manoharan, P. Nordlander, G. Shvets and F. Capasso, *Science*, 2010, **328**, 1135–1138.
5 G. Lee, Y.-S. Cho, S. Park and G.-R. Yi, *Korean J. Chem. Eng.*, 2011, **28**, 1641–1650.
6 Q. Chen, S. C. Bae and S. Granick, *Nature*, 2011, **469**, 381–384.
7 L. Rossi, S. Sacanna, W. T. M. Irvine, P. M. Chaikin, D. J. Pine and A. P. Philipse, *Soft Matter*, 2011, **7**, 4139.
8 D. V. Talapin, E. V. Shevchenko, M. I. Bodnarchuk, X. Ye, J. Chen and C. B. Murray, *Nature*, 2009, **461**, 964–967.
9 D. Zerrouki, J. Baudry, D. Pine, P. Chaikin and J. Bibette, *Nature*, 2008, **455**, 380–382.
10 T. Gibaud, E. Barry, M. J. Zakhary, M. Henglin, A. Ward, Y. Yang, C. Berciu, R. Oldenbourg, M. F. Hagan, D. Nicastro, R. B. Meyer and Z. Dogic, *Nature*, 2012, 1–6.
11 S. Sacanna, W. T. M. Irvine, P. M. Chaikin and D. J. Pine, *Nature*, 2010, **464**, 575–578.
12 D. J. Kraft, R. Ni, F. Smallenburg, M. Hermes, K. Yoon, D. A. Weitz, A. van Blaaderen, J. Groenewold, M. Dijkstra and W. K. Kegel, *Proc. Natl. Acad. Sci. U. S. A.*, 2012, **109**, 10787–10792.
13 L. Wang and L. Gao, *J. Colloid Interface Sci.*, 2010, **349**, 519–526.
14 M. Motornov, S. Z. Malynych, D. S. Pippalla, B. Zdyrko, H. Royter, Y. Roiter, M. Kahabka, A. Tokarev, E. Zhulina, K. G. Kornev, I. Luzinov and S. Minko, *Nano Lett.*, 2012, **12**, 3814–3820.
15 S. Sacanna, L. Rossi and D. J. Pine, *J. Am. Chem. Soc.*, 2012, **134**, 6112–6115.
16 S. Kantorovich, R. Weeber, J. J. Cerda and C. Holm, *Soft Matter*, 2011, **7**, 5217.
17 M. Klinkigt, R. Weeber, S. Kantorovich and C. Holm, *Soft Matter*, 2011, **9**, 3535.
18 M. Piastra and E. G. Virga, *Soft Matter*, 2012, **8**, 10960.
19 E. C. Gartland, Jr and E. G. Virga, *Soft Matter*, 2013, **9**, 5991.
20 M. P. Allen and D. J. Tildesley, *Computer Simulations of Liquids*, Oxford University Press, Oxford, England, 1987.
21 P. Linse, in *Adv. Poly. Sci.*, ed. C. Holm and K. Kremer, Springer, Berlin, 2005, vol. 185.
22 W. H. Press, B. P. Flannery, S. A. Teukolsky and W. V. Vetterling, *Numerical Recipes. The art of Scientific Computing*, Cambridge University Press, Cambridge, England, 1986.